C. R. Mecanique 342 (2014) 326–333

Contents lists available at ScienceDirect

Comptes Rendus Mecanique

www.sciencedirect.com

Frontiers of micro and nanomechanics of materials: Soft or amorphous matter, surface effects

A stochastic homogenization approach to estimate bone elastic properties

Une approche d'homogénéisation stochastique pour estimer les propriétés élastiques de l'os

Vittorio Sansalone [a,b,*], Salah Naili [a,b], Christophe Desceliers [b]

[a] *Université Paris-Est, Laboratoire Modélisation et Simulation Multi-Échelle, MSME UMR 8208 CNRS, 61, Av. du Général de Gaulle, 94010 Créteil, France*

[b] *Université Paris-Est, Laboratoire Modélisation et Simulation Multi-Échelle, MSME UMR 8208 CNRS, 5, bd Descartes, 77454 Marne-la-Vallée, France*

ARTICLE INFO

Article history:
Received 31 May 2013
Accepted after revision 10 December 2013
Available online 1 May 2014

Keywords:
Biomechanics
Continuum micromechanics
Stochastic modeling
Maximum entropy principle
Elastic properties

Mots-clés :
Biomécanique
Micromécanique des milieux continus
Modélisation stochastique
Principe du maximum d'entropie
Propriétés élastiques

ABSTRACT

The mechanical properties of bone tissue depend on its hierarchical structure spanning many length scales, from the organ down to the nanoscale. Multiscale models allow estimating bone mechanical properties at the macroscale based on information on bone organization and composition at the lower scales. However, the reliability of these estimates can be questioned in view of the many uncertainties affecting the information which they are based on. In this paper, a new methodology is proposed, coupling probabilistic modeling and micromechanical homogenization to estimate the material properties of bone while taking into account the uncertainties on the bone micro- and nanostructure. Elastic coefficients of bone solid matrix are computed using a three-scale micromechanical homogenization method. A probabilistic model of the uncertain parameters allows propagating the uncertainties affecting their actual values into the estimated material properties of bone. The probability density functions of the random variables are constructed using the Maximum Entropy principle. Numerical simulations are used to show the relevance of this approach.

RÉSUMÉ

Les propriétés mécaniques du tissu osseux dépendent de sa structure hiérarchisée, de l'échelle de l'organe à celle de ses constituants élémentaires (nano-échelle). En se basant sur la connaissance de la morphologie, de l'organisation et des propriétés mécaniques de ces derniers, des modèles multi-échelles permettent d'estimer les propriétés mécaniques d'ensemble du tissu osseux. Cependant, ces informations sont souvent partielles ou incertaines, rendant peu fiables lesdites estimations. Dans cet article, nous proposons une stratégie originale permettant de prendre en compte ces difficultés de façon efficace. Plus précisément, un modèle multi-échelles du tissu osseux basé sur la théorie de la micromécanique des milieux continus est associé à un traitement probabiliste de certaines des variables du modèle (notamment, les propriétés mécaniques des constituants

* Corresponding author.
E-mail address: vittorio.sansalone@univ-paris-est.fr (V. Sansalone).

http://dx.doi.org/10.1016/j.crme.2013.12.007
1631-0721/

élémentaires du tissu osseux). Le modèle multi-échelle permet de prendre en compte la microarchitecture et l'organisation du tissu osseux aux petites échelles pour estimer les coefficients élastiques de l'ultrastructure osseuse (la matrice solide du tissu osseux). Les incertitudes sur les variables d'entrée sont prises en compte en construisant des lois de probabilités pertinentes basées sur le principe du maximum d'entropie. Quelques résultats numériques sont montrés pour étayer l'intérêt de cette approche.

1. Introduction

Bone is a biocomposite material showing several levels of microstructural organization [1]. In mature bone, two types of tissues can be distinguished: cortical tissue—a dense material forming the outer shell of bones—, and trabecular tissue—a spongy material located inside the bone. Both cortical and trabecular tissues are porous materials. Pores in cortical bones are pseudo-cylindrical canals (Havers' and Volkmann's canals), whereas, in trabecular bone, pores are irregularly shaped cavities. Despite the very different pore morphology, the solid matrix of both cortical and trabecular tissues, hereafter referred to as bone *ultrastructure*, is nearly the same. Bone ultrastructure is an assembly of mineralized collagen fibrils (MCF). MCF are bunches of collagen molecules embedded in a mineral-rich matrix. This latter is made of hydroxyapatite mineral and constitutional water.

Understanding bone mechanical properties requires accounting for its hierarchical structure down to the lowest levels of this hierarchy [2,3]. Multiscale modeling and simulation turns out to be a powerful tool for explaining bone mechanical properties while accounting for its inner organization.

Several authors studied bone focusing on several levels of its hierarchical structure by means of multiscale modeling approaches [4–7]. Modeling studies rely on the experimental characterization of bone microstructure obtained through different experimental techniques (ultrasounds, X-ray microtomography (micro-CT), X-ray synchrotron radiation, etc.) aiming at relating the available clinically relevant information to bone mechanical properties. Several experimental studies highlighted the relevance of porosity and mineralization in determining the mechanical properties of bone and the associated fracture risk [8–15]. Recently, the heterogeneous distribution of bone elastic coefficients in the inferior human femoral neck was described using a continuum micromechanics model based on 3D mappings of porosity and Tissue Mineral Density (TMD) obtained through high-resolution synchrotron radiation [16,17,7].

A critical point for clinical application of biomechanical models of bone is the incomplete knowledge of patient-specific information on bone microstructure. Techniques such as ultrasounds and micro-CT, commonly used in in vivo measurements, can hardly inspect bone microstructure at the sub-micrometric scale. Moreover, the information which is actually made available by the different experimental techniques is affected by the resolution and parameterization of the experimental setup. Furthermore, some of the uncertain parameters may be not directly available from experimental measures but have to be deduced by introducing additional empirical relationships. All these issues may affect the accuracy of the modeling parameters used to estimate bone mechanical properties, questioning the reliability of the model predictions.

Uncertainties on the modeling parameters increase with zooming down into the nanostructure of bone. Current experimental techniques cannot provide accurate information about the morphology, spatial arrangement and mechanical behavior of bone constituents. Not surprisingly, modeling assumptions at the nanoscale may be very different. For instance, bone nanostructure has been described as either a mineral-rich matrix embedding collagen molecules [4,5,16] or as a collagen matrix with mineral inclusions [18–22].

We propose to cope with these experimental limitations by developing a novel multiscale model of bone taking into account the uncertainties on bone nanostructure. A multiscale model will make the global elastic behavior of bone emerge by combining models developed at each relevant scale of bone microstructure. A probabilistic model will allow accounting for the uncertainties about the patient-specific microstructure and to propagate them up to the organ scale. In this very first study, we will focus only on the uncertainties affecting the elastic properties of bone constituents.

Similar approaches have been used to model effective mechanical properties of materials with random microstructure (see for instance [23,24]). Nevertheless, to the best of our knowledge, this is the very first contribution to develop a stochastic modeling of bone.

In order to construct the probabilistic model of bone, we combined a multiscale model based on continuum micromechanics [25,26] with a probabilistic representation of the uncertain parameters of the model, based on the Maximum Entropy principle [27,28]. The paper is organized as follows. The multiscale model of bone based on the continuum micromechanics theory is resumed in Section 2. The probabilistic model of the uncertain parameters is described in Section 3. The numerical procedure and some numerical results are presented in Section 4 to highlight the features of this approach. Eventually, the conclusions of this study are drawn in Section 5 opening the way to further research.

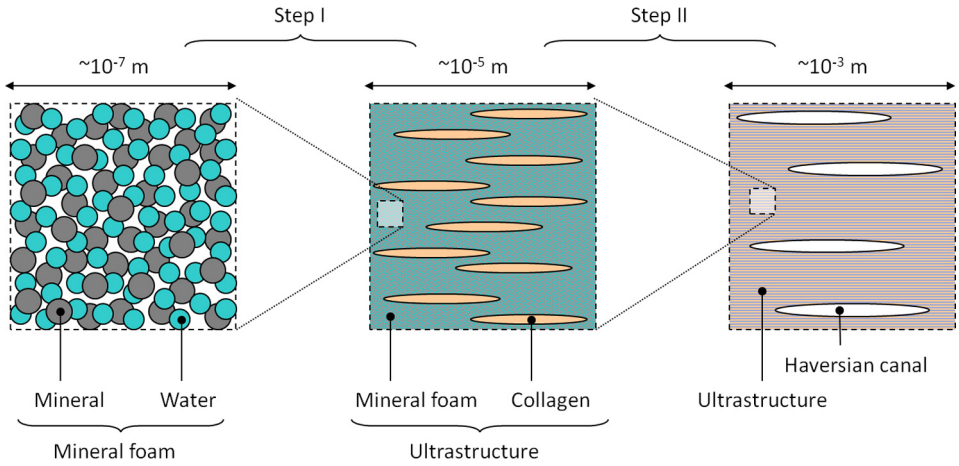

Fig. 1. (Color online.) Two-step homogenization to compute the effective elastic properties of bone ultrastructure. Bone ultrastructure is the solid matrix of bone tissue, surrounding the Haversian and Volkmann canals.

2. Mean continuum micromechanics model of bone ultrastructure

In view of our target application, we will refer only to elasticity problems. Hereafter, micromechanical homogenization will refer to the homogenization strategy based on the theory of continuum micromechanics. Continuum micromechanics allow estimating the effective elastic properties of a material with microstructure based on the knowledge of the nature and arrangement of its constituent phases [26,25,29]. Estimates of the homogenized elasticity tensor $\mathbb{c}_{\text{hom}}$ of a material with microstructure of matrix-inclusion type are obtained based on the solution of the matrix-inclusion problem provided by Eshelby in the 1950s [30] and further extensions [31]. The estimated homogenized elasticity tensor $\mathbb{c}_{\text{hom}}$ is thus provided by:

$$\mathbb{c}_{\text{hom}} = \sum_r f_r \, \mathbb{c}_r : \left(\mathbb{i} + \mathbb{p}_r^0 : (\mathbb{c}_r - \mathbb{c}_0)\right)^{-1} : \left(\sum_s f_s \left(\mathbb{i} + \mathbb{p}_s^0 : (\mathbb{c}_s - \mathbb{c}_0)\right)^{-1}\right)^{-1} \tag{1}$$

where f_r is the volume fraction of phase r ($\sum_r f_r = 1$), $\mathbb{i}$ is the 4th-order symmetric identity tensor, $\mathbb{c}_r$ is the elasticity tensor of phase r, $\mathbb{c}_0$ is the elasticity tensor of the "effective matrix" (hereafter referred to by sub/superscript "0") where the phases are embedded, and $\mathbb{p}_r^0$ is the so-called Hill tensor of phase/inclusion r embedded in the effective matrix. The Hill tensor accounts for the characteristic shape of the inclusions constituting the phase r in the effective matrix. The choice of $\mathbb{c}_0$, i.e. of the effective matrix, leads to different estimates of $\mathbb{c}_{\text{hom}}$. Among others, two estimates are relevant to our context. The Mori–Tanaka (MT) estimate [25] applies when an actual "matrix" phase can be identified. Thus, the effective matrix is the actual matrix phase ($\mathbb{c}_0 = \mathbb{c}_{\text{matrix}}$). The Self-Consistent (SC) estimate [25] is well suited when no actual matrix can be identified, but the microstructure is rather made of interpenetrating phases. In this case, the effective matrix is assumed to be the homogenized material itself ($\mathbb{c}_0 = \mathbb{c}_{\text{hom}}$). Hereafter, $\mathbb{c}_{\text{hom}}^{\text{MT}}$ and $\mathbb{c}_{\text{hom}}^{\text{SC}}$ will refer to the MT and SC estimates of $\mathbb{c}_{\text{hom}}$, respectively. Note that Eq. (1) can be rewritten as:

$$g(\mathbb{c}_{\text{hom}}; f, w) = 0 \tag{2}$$

which can be solved for $\mathbb{c}_{\text{hom}}$ based on the sets of the volume fractions and of independent elastic coefficients of the phases, noted f and w, respectively.

2.1. Application to bone ultrastructure

Bone is a multiscale material basically constituted of collagen, minerals, and water. (Other bone constituents, such as non-collagenous organic molecules, are here disregarded.) A detailed representation of the hierarchical organization of bone and of its description in the scope of continuum micromechanics can be found in [4]. We will concern ourselves with estimating the elastic properties of bone ultrastructure. Following the "Concept I" of [32], we will consider three relevant scales, see Fig. 1. First, at the scale of a few millimeters (scale of the tissue), bone ultrastructure constitutes the solid matrix of bone tissue surrounding the Haversian and Volkmann canals (schematically depicted on the right of Fig. 1 by white, elongated pores). Second, at the scale of a few tens of micrometers (scale of the ultrastructure), bone ultrastructure is seen as an assembly of mineralized collagen fibrils, where collagen molecules (300 nm long) are embedded in a mineral-rich matrix referred to as mineral foam. Eventually, at the scale of few hundred nanometers (scale of the mineral foam), the mineral foam is seen as a highly disordered mixture of hydroxyapatite minerals and constitutional water particles. This representation of the hierarchical organization of bone requires two homogenization steps to compute the effective properties of bone ultrastructure. First, the effective elastic properties of the mineral foam will be computed as a mixture of mineral and water (step I). Then, the effective elastic properties of the ultrastructure will be computed considering collagen inclusions in the mineral foam (step II).

2.1.1. Step I: effective elasticity tensor of the mineral foam

At the scale of a few hundred nanometers (Fig. 1, on the left), highly disordered hydroxyapatite crystals interpenetrated by water-filled spaces form a mineral foam. The disordered structure observable at this scale [33] motivates the use of a Self-Consistent scheme to estimate the homogenized tensor of the mineral foam ($\mathbb{c}_{\text{foam}}$). Both mineral and water were modeled as spherical particles with isotropic elastic behavior. The elastic tensor of the mineral was parameterized by its Young modulus y_{HA} and its Poisson coefficient ν_{HA}. The elastic tensor of the water was parameterized by its bulk modulus k_{w} (shear modulus $g_{\text{w}} = 0$). The corresponding mixture is isotropic. Thus, Eq. (2) becomes:

$$g_{\text{I}}(\mathbb{c}_{\text{foam}};\, f_{\text{I}},\, w_{\text{I}}) = 0 \tag{3}$$

where $f_{\text{I}} \equiv f_{\text{HA}}^{\text{foam}}$ is the volume fraction of the mineral in the foam and the vector w_{I} collects the elastic parameters of the constituent phases: $w_{\text{I}} = (y_{\text{HA}}, \nu_{\text{HA}}, k_{\text{w}})$. Eq. (3), encoding a Self-Consistent solution scheme, turns out to be an implicit function of $\mathbb{c}_{\text{foam}}$ which has to be computed iteratively. Note that $\mathbb{c}_{\text{foam}}$ can be parameterized by the Young modulus y_{foam} and the Poisson coefficient ν_{foam} of the mineral foam.

2.1.2. Step II: effective elasticity tensor of the ultrastructure

At the scale of several micrometers (Fig. 1, in the middle), collagen molecules are embedded into the mineral foam. The elongated form of collagen molecules and the contiguity of the mineral phase leads to the use of a Mori–Tanaka scheme to estimate the homogenized elastic tensor of the ultrastructure ($\mathbb{c}_{\text{ultra}}$). Thus, the matrix phase is the (isotropic) mineral foam described in step I and the collagen is modeled as cylindrical inclusions. For the sake of simplicity, the collagen was considered as an isotropic material whose elastic tensor was parameterized by the Young modulus y_{col} and the Poisson coefficient ν_{col}. The mixture obtained is transversely isotropic. Thus, Eq. (2) becomes:

$$g_{\text{II}}(\mathbb{c}_{\text{ultra}};\, f_{\text{II}},\, w_{\text{II}}) = 0 \tag{4}$$

where $f_{\text{II}} \equiv f_{\text{col}}^{\text{ultra}}$ is the volume fraction of the collagen in the ultrastructure and the vector w_{II} collects the independent elastic parameters of the collagen and of the mineral foam: $w_{\text{II}} = (y_{\text{col}}, \nu_{\text{col}}, y_{\text{foam}}, \nu_{\text{foam}})$. In particular, y_{foam} and ν_{foam} are extracted from the tensor $\mathbb{c}_{\text{foam}}$ computed in step I. Eq. (4), encoding a Mori–Tanaka solution scheme, can be explicitly solved for $\mathbb{c}_{\text{ultra}}$.

3. Probabilistic multiscale model of bone

3.1. Probabilistic model of the uncertain parameters of the multiscale bone model

Using deterministic models, such as the mean continuum micromechanics model of bone ultrastructure, assumes that the mechanical properties of the constituents at the microscale are well identified. This requires some experimental measurements at the microscale which can be tricky to be carried out. Consequently, most of the time, information concerning the elastic properties at the microscale is uncertain. There exist several approaches in order to take into account such uncertainties among which the theory of probability [34–37] has proved, during last decades, its efficiency and its robustness. In the framework of a parametric probabilistic approach, uncertainties on the constituents at the microscale are taken into account by modeling the uncertain elastic properties by random variables or by random fields. The uncertainties on a generic parameter x of the model (Young modulus, Poisson coefficient, etc.) is modeled in substituting x by a real-valued random variable X. Hereinafter, it is assumed that the probability law of X is defined by a probability density function $x \mapsto p_X(x)$ on $\mathbb{R}$. The construction of the probability law of the random variables must be carefully carried out because the probability distributions embed statistical information that must be in accordance with the properties of the mathematical operators of the boundary value problems involving X and with the values of any given statistical quantities of X [38,39]. Any arbitrary construction of the probabilistic model of X would result in a non-correct probabilistic model of the random effective elastic tensors. In this paper, the construction of a probabilistic model is carried out in using the MaxEnt principle [40,41,27,28,42,43]. Hereinafter, we assume that uncertainties only concern a few elastic properties of the mechanical model introduced in Section 2.1. Concerning the collagen and the mineral, the Young moduli and the Poisson coefficients are uncertain. Concerning the water, bulk modulus is uncertain. In the following sections, the probability density functions of the random variables modeling these uncertain parameters are presented.

3.1.1. Probabilistic model of the Young moduli and the bulk modulus

For all $r \in \{\text{col}, \text{HA}\}$, the uncertain Young modulus y_r is modeled by a random variable Y_r with probability density function p_{Y_r}. The uncertain bulk modulus k_{w} of water is modeled by a random variable K_{w} with probability density function $p_{K_{\text{w}}}$. Let X be either Y_r or K_{w}. The available information is the following: (*i*) the support of X is $\mathcal{S}_X = [0, +\infty[$; (*ii*) the mean value of X is m_X; (*iii*) the ellipticity property of the elasticity tensor implies that $E(1/X^2) < +\infty$ (see [44]) where $E(\cdot)$ is the mathematical expectation operator. It can be shown that the MaxEnt principle with the constraints of information (*i*)–(*iii*) yields

$$p_X(x) = \mathbb{1}_{[0,+\infty[}(x)\, c_X\, x^{(1-(\delta_X)^2)/(\delta_X)^2}\, \exp\left(-\frac{x}{m_X\,(\delta_X)^2}\right), \quad \text{with } c_X = m_X\,(\delta_X)^{-\frac{(\delta_X)^2}{2}} / \Gamma\left((\delta_X)^{-2}\right) \tag{5}$$

where $x \mapsto \Gamma(x)$ is the Gamma function. Note that p_X depends on the mean value m_X and on the dispersion $\delta_X = \sigma_X/m_X$ of X, with σ_X^2 the variance of X.

3.1.2. Probabilistic model of the Poisson ratios

For all $r \in \{\text{col}, \text{HA}\}$, the uncertain Poisson ratio v_r is modeled by a random variable V_r with a probability density function p_{V_r}. The available information is: (*i*) the support $\mathcal{S}_{V_r} =]-1, 1/2[$; (*ii*) the mean value m_{V_r}; (*iii*) the integrability condition $E((1-V_r)^2/(1+V_r)^2(1-2V_r)^2) < +\infty$. Information (*iii*) follows from requiring the second-order moments of the wave velocities to be finite [45]. Then, use of the MaxEnt principle with the constraints of information (*i*)–(*iii*) yields:

$$p_{V_r}(x) = \mathbb{1}_{]-1,1/2[}(x) \exp\left(-\lambda_0 - \lambda_1 x - \lambda_2 \frac{(1-x)^2}{(1+x)^2(1-2x)^2}\right) \tag{6}$$

where parameters λ_0, λ_1 and λ_2 are obtained by solving the following system of equations:

$$\int_{-1}^{1/2} x \exp\left(-\lambda_0 - \lambda_1 x - \lambda_2 \frac{(1-x)^2}{(1+x)^2(1-2x)^2}\right) \mathrm{d}x = m_{V_r} \tag{7}$$

$$\int_{-1}^{1/2} x^2 \exp\left(-\lambda_0 - \lambda_1 x - \lambda_2 \frac{(1-x)^2}{(1+x)^2(1-2x)^2}\right) \mathrm{d}x = (m_{V_r})^2(\delta_{V_r})^2 + (m_{V_r})^2 \tag{8}$$

$$\int_{-1}^{1/2} \exp\left(-\lambda_0 - \lambda_1 x - \lambda_2 \frac{(1-x)^2}{(1+x)^2(1-2x)^2}\right) \mathrm{d}x = 1 \tag{9}$$

Note that the values of λ_0, λ_1 and λ_2 depend on the mean value m_{V_r} and the dispersion coefficient δ_{V_r} of V_r.

3.2. Probabilistic multiscale model of bone

The probabilistic multiscale bone model is constructed by substituting the vectors of parameters $w_{\text{I}} = (y_{\text{HA}}, v_{\text{HA}}, k_{\text{w}})$ and $w_{\text{II}} = (y_{\text{col}}, v_{\text{col}}, y_{\text{foam}}, v_{\text{foam}})$ by the random vectors $W_{\text{I}} = (Y_{\text{HA}}, V_{\text{HA}}, K_{\text{w}})$ and $W_{\text{II}} = (Y_{\text{col}}, V_{\text{col}}, Y_{\text{foam}}, V_{\text{foam}})$ in Eq. (3) (homogenization step I) and Eq. (4) (homogenization step II), respectively. Then we have:

$$g_{\text{I}}(\mathbb{C}_{\text{foam}}; f_{\text{I}}, W_{\text{I}}) = 0 \quad \text{and} \quad g_{\text{II}}(\mathbb{C}_{\text{ultra}}; f_{\text{II}}, W_{\text{II}}) = 0 \tag{10}$$

Since W_{I} and W_{II} are random variables, tensors $\mathbb{C}_{\text{foam}}$ and $\mathbb{C}_{\text{ultra}}$ turn out to be random variables as well.

The Monte Carlo numerical method is used in order to solve the system of stochastic equations of Eq. (10). First, for each statistically independent realizations $W_{\text{I}}(a_1), \ldots, W_{\text{I}}(a_N)$, statistically independent realizations $\mathbb{C}_{\text{foam}}(a_1), \ldots, \mathbb{C}_{\text{foam}}(a_N)$ of random tensor $\mathbb{C}_{\text{foam}}$ are calculated by solving the N following equations successively:

$$g_{\text{I}}\big(\mathbb{C}_{\text{foam}}(a_1); f_{\text{I}}, W_{\text{I}}(a_1)\big) = 0 \quad \ldots \quad g_{\text{I}}\big(\mathbb{C}_{\text{foam}}(a_N); f_{\text{I}}, W_{\text{I}}(a_N)\big) = 0 \tag{11}$$

Then, statistically independent realizations $\mathbb{C}_{\text{ultra}}(a_1), \ldots, \mathbb{C}_{\text{ultra}}(a_N)$ of random tensor $\mathbb{C}_{\text{ultra}}$ are calculated by solving the N following equations successively

$$g_{\text{II}}\big(\mathbb{C}_{\text{ultra}}(a_1); f_{\text{II}}, W_{\text{II}}(a_1)\big) = 0 \quad \ldots \quad g_{\text{II}}\big(\mathbb{C}_{\text{ultra}}(a_N); f_{\text{II}}, W_{\text{II}}(a_N)\big) = 0 \tag{12}$$

Statistics on $\mathbb{C}_{\text{foam}}$ and $\mathbb{C}_{\text{ultra}}$ are then estimated as the corresponding statistics of $\mathbb{C}_{\text{foam}}(a_1), \ldots, \mathbb{C}_{\text{foam}}(a_N)$ and $\mathbb{C}_{\text{ultra}}(a_1), \ldots, \mathbb{C}_{\text{ultra}}(a_N)$.

The solution algorithm, implemented in Matlab code, is schematically depicted in Fig. 2.

4. Numerical results and discussion

The Monte Carlo numerical simulation has been carried out for mean values of the parameters given in [19]. Three different values of the dispersion coefficients of the random variables (assumed to be the same for each one) were used, namely 0.05, 0.1, and 0.2. Volume fractions are free parameters (f.p.s) of the model. Values typical of mature, fully mineralized bone were chosen, namely $f_{\text{I}} \equiv f_{\text{HA}}^{\text{foam}} = 0.9$ and $f_{\text{II}} \equiv f_{\text{col}}^{\text{ultra}} = 0.5$. All the numerical simulations were performed using a custom Matlab code.

For $N = 10^4$ statistically independent realizations and with dispersion coefficients equal to $\delta = 0.2$ (for each random variable), the relative error between the mean values of the statistically independent realizations and the mean values of the random variable was lower than 0.1% for any random variable (but V_{col}, for which this error was 0.2%). Moreover, the relative error between the dispersion of the realizations and the dispersion of the random variables was lower than

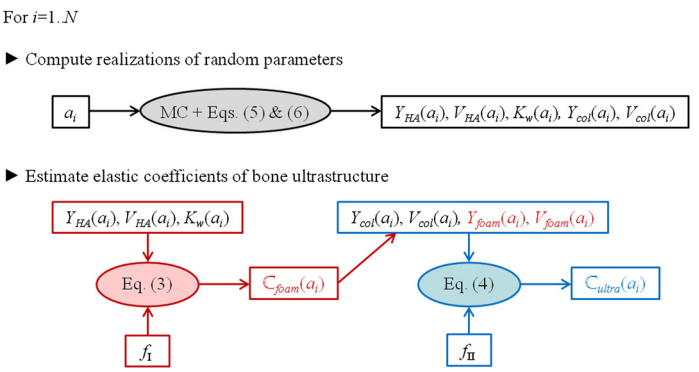

Fig. 2. (Color online.) Algorithm used for solving the stochastic multiscale model.

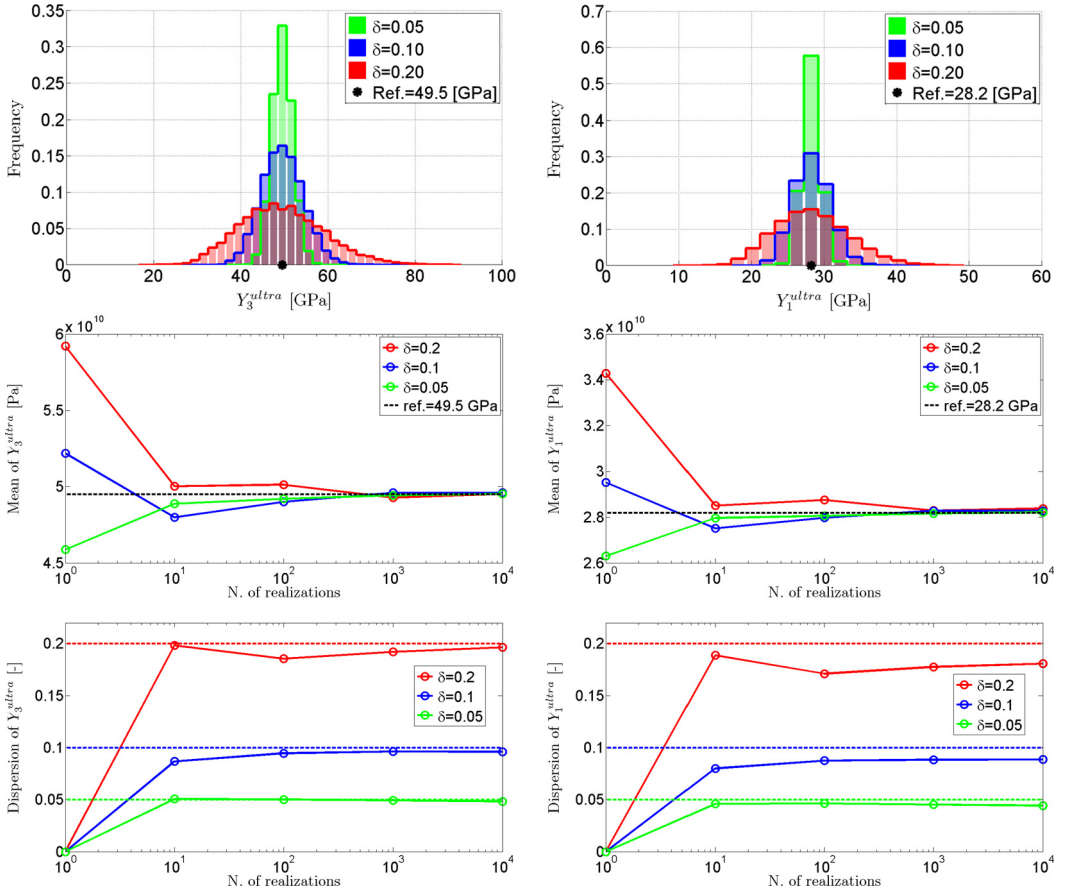

Fig. 3. Statistically independent realizations (on the top), mean values (in the middle) and dispersion coefficient (on the bottom) of the axial modulus of bone ultrastructure in the direction of the osteonal axis (on the left) and in the isotropy plane (on the right) as a function of the number of realizations. Green, blue, and red markers and lines correspond to a dispersion $\delta = 0.05, 0.1$, and 0.2, respectively, of the uncertain parameters. See text for details on the other input data. (For interpretation of the references to color in this figure, the reader is referred to the web version of this article.)

1.0% for each random variable (but Y_{HA}, for which this error was 1.3%). Then, the statistically independent realizations $\mathbb{C}_{\mathrm{foam}}(a_1), \ldots, \mathbb{C}_{\mathrm{foam}}(a_N)$ and $\mathbb{C}_{\mathrm{ultra}}(a_1), \ldots, \mathbb{C}_{\mathrm{ultra}}(a_N)$ were constructed using the multiscale procedure described in Section 2. In Fig. 3, results concerning the axial modulus of bone ultrastructure in the direction of the osteonal axis (Y_3^{ultra}, on the left) and in the transverse isotropy plane (Y_1^{ultra}, on the right) are shown. Results obtained for the other elastic coefficients show a similar trend (data not shown). Throughout Fig. 3, green, blue, and red markers and lines refer to $\delta = 0.05, 0.1$, and 0.2, respectively.

The probability density functions Y_3^{ultra} and Y_1^{ultra} are estimated and shown on the top row of Fig. 3. Black markers refer to the values y_3^{ultra} and y_1^{ultra} of the axial modulus of bone ultrastructure in the direction of the osteonal axis and in

the isotropy plane, respectively, calculated by using the mean continuum micromechanics model. Statistically independent realizations of Y_3^{ultra} and Y_1^{ultra} are distributed around their corresponding mean values irrespective of their dispersion coefficient δ, spreading out as δ increases. Note that positiveness of the axial elastic moduli follows from the probabilistic model constructed in the previous section. Relevant statistics of these distributions are shown in the central and bottom rows of Fig. 3. In the central row of Fig. 3, estimates of the mean values of the statistically independent realizations of Y_3^{ultra} and Y_1^{ultra} (colored solid lines) are shown as a function of the number of realizations. The values y_3^{ultra} and y_1^{ultra}, calculated by the mean continuum micromechanics model, are depicted by black dashed lines. In the bottom row of Fig. 3, the dispersion coefficients of the statistical realizations of Y_3^{ultra} and Y_1^{ultra} (colored solid lines) are shown as a function of the number of realizations. Dispersion coefficients of the uncertain parameters are depicted by colored dashed lines. Two effects are remarkable. First, it can be observed that y_3^{ultra} *and* y_1^{ultra} *are a good approximation of the mean values of* Y_3^{ultra} *and* Y_1^{ultra}. Second, the dispersions coefficients of Y_3^{ultra} and Y_1^{ultra} are not equal to the values of the dispersion coefficients of the uncertain parameters. Interestingly, the dispersion coefficients of both Y_3^{ultra} and Y_1^{ultra} are smaller than those of the random variables modeling the uncertain parameters. Therefore, *the statistical fluctuations of the elastic coefficients of bone are smaller than those of its elementary constituents*. We repeated the same calculations for several values of the volume fractions and obtained always the same trend. This proves the generality of the above conclusions.

5. Conclusions

Lack of patient-specific data and uncertainties affecting available in vivo and in vitro information in bone, especially at the small scales of its hierarchical structure, may question the reliability of results provided by multiscale models that use these data to estimate upper-scale properties of bone. The probabilistic multiscale model proposed in this paper aims at overcoming these difficulties by estimating bone mechanical properties based on a few available data while preserving robustness of modeling. Suitable probabilistic models for the uncertain parameters are built based on the information that is actually available (of either experimental or theoretical nature). Therefore, uncertainties affecting the modeling parameters at the lower scales of bone hierarchy are propagated at the upper scale, ending up with numerically computed probability density functions of the elastic moduli of bone. Inspection of these results brings out two aspects. First, it is suggested that the mean model provides good approximations of the mean values of the elastic properties of bone. Moreover, the statistical fluctuations of the latter are smaller than those of the uncertain parameters, suggesting that the effects of the uncertainties decrease when calculating the effective properties of bone.

The proposed stochastic multiscale modeling approach also allows computing confidence intervals or bounds. Other methods exist to compute bounds on the effective parameters. For instance, the use of the Worst Scenario approach would allow calculating a deterministic value of the effective parameters bounds, whenever these bounds do exist, in carrying out an adapted interval analysis for each parameter of the mean model. Nevertheless, such a method does not allow propagating the uncertainties from the lower scale to the upper scales. This is why a probabilistic approach has been used to construct the probability density function, or the statistics, related to the effective parameters, including the random bounds.

To conclude, a few remarks on the scope and limitations of the proposed modeling strategy are in order. Effectiveness of continuum micromechanics in modeling bone elastic properties has been proved by Hellmich and co-workers using independent sets of experiments (see, e.g., [32]). The basic requirement of multiscale modeling is the so-called scale-separation principle. This requirement is fulfilled by the three scales considered in this study, see Fig. 1. Besides that, numerical results are affected by the modeling assumptions at the different scales. The key ingredients of the model are the relative amount, shape, and elastic behavior of the constituent phases (collagen, mineral, and water). On the one hand, elastic coefficients were modeled as random variables. Indeed, elastic coefficients are actually *effective* parameters representing *both* the elasticity of the constituent phases *and* the interactions between them. Randomness in their values accounts for the imperfect knowledge of the effective elastic behavior of bone constituents at the nanoscale which is affected by size effects, cross-link density, phase-to-phase imperfect adhesion, and so forth. That being the case, the effective elastic coefficients are actually uncertain parameters of the model and were therefore treated as random variables. On the other hand, relative amount and shape of constituent phases were treated as free parameters. Volume fractions of bone constituents are supposed to be known through experimental measurements. Although morphological information on collagen is well acknowledged (step II, Section 2.1.2), current experimental techniques do not allow one to retrieve accurate information about the morphology of mineral and water particle in the mineral foam (step I, Section 2.1.1) which were therefore modeled as spherical particles. Aiming at patient specific modeling, modeling of both amount and morphology of bone constituents needs to be improved. In a forthcoming work, we will develop a stochastic treatment of the amount and shape parameterization of bone constituents in order to take into account the incomplete, patient-specific information available through current in vivo devices.

A last issue concerns the validity of continuum modeling of the mineral foam (step I, Section 2.1.1). Indeed, continuum mechanics may break down at length scales lower than about a hundred nanometers (the characteristic length of the RVE of the mineral foam, see Fig. 1) and molecular modeling should be used instead. However, the wealth of information needed by molecular modeling approaches is completely missing at the current state of knowledge. Continuum mechanics somehow filters out most of these nanoscopic details and is likely to provide a reasonable accurate modeling of the system.

References

[1] S.C. Cowin (Ed.), Bone Mechanics Handbook, CRC Press, Boca Raton, FL, USA, 2001.
[2] D.J. Hulmes, Building collagen molecules, fibrils, and suprafibrillar structures, J. Struct. Biol. 137 (2002) 2–10.
[3] P. Fratzl, H.S. Gupta, E.P. Paschalis, P. Roschger, Structure and mechanical quality of the collagen–mineral nano-composite in bone, J. Mater. Chem. 14 (2004) 2115–2123.
[4] A. Fritsch, C. Hellmich, 'Universal' microstructural patterns in cortical and trabecular, extracellular and extravascular bone materials: micromechanics-based prediction of anisotropic elasticity, J. Theor. Biol. 244 (4) (2007) 597–620.
[5] M. Predoi-Racila, J.-M. Crolet, Human cortical bone: the SiNuPrOs model, Comput. Methods Biomech. Biomed. Eng. 11 (2) (2008) 169–187.
[6] W.J. Parnell, M.B. Vu, Q. Grimal, S. Naili, Analytical methods to determine the effective mesoscopic and macroscopic elastic properties of cortical bone, Biomech. Model. Mechanobiol. 11 (6) (2012) 883–901.
[7] V. Sansalone, V. Bousson, S. Naili, C. Bergot, F. Peyrin, J.D. Laredo, G. Haiat, Effects of the axial variations of porosity and mineralization on the elastic properties of the human femoral neck, Comput. Model. Eng. Sci. 87 (5) (2012) 387–409.
[8] J.D. Currey, The effect of porosity and mineral content on the Young's modulus of elasticity of compact bone, J. Biomech. 21 (2) (1988) 131–139.
[9] K.L. Bell, N. Loveridge, J. Power, N. Garrahan, B.F. Meggitt, J. Reeve, Regional differences in cortical porosity in the fractured femoral neck, Bone 24 (1) (1999) 57–64.
[10] E.G. Vajda, R.D. Bloebaum, Age-related hypermineralization in the female proximal human femur, Anat. Rec. 255 (2) (1999) 202–211.
[11] V. Bousson, A. Meunier, C. Bergot, E. Vicaut, M.A. Rocha, M.H. Morais, A.M. Laval-Jeantet, J.D. Laredo, Distribution of intracortical porosity in human midfemoral cortex by age and gender, J. Bone Miner. Res. 16 (7) (2001) 1308–1317.
[12] N. Crabtree, N. Loveridge, M. Parker, N. Rushton, J. Power, K.L. Bell, T.J. Beck, J. Reeve, Intracapsular hip fracture and the region-specific loss of cortical bone: analysis by peripheral quantitative computed tomography, J. Bone Miner. Res. 16 (7) (2001) 1318–1328.
[13] D.B. Burr, Bone quality: understanding what matters, J. Musculoskelet. Neuronal Interact. 4 (2) (2004) 184–186.
[14] M. Sasso, G. Haiat, Y. Yamato, S. Naili, M. Matsukawa, Dependence of ultrasonic attenuation on bone mass and microstructure in bovine cortical bone, J. Biomech. 41 (2) (2008) 347–355.
[15] R.M. Zebaze, A. Ghasem-Zadeh, A. Bohte, S. Iuliano-Burns, M. Mirams, R.I. Price, E.J. Mackie, E. Seeman, Intracortical remodelling and porosity in the distal radius and post-mortem femurs of women: a cross-sectional study, Lancet 375 (9727) (2010) 1729–1736.
[16] V. Sansalone, S. Naili, V. Bousson, C. Bergot, F. Peyrin, J. Zarka, J.D. Laredo, G. Haiat, Determination of the heterogeneous anisotropic elastic properties of human femoral bone: from nanoscopic to organ scale, J. Biomech. 43 (10) (2010) 1857–1863.
[17] V. Sansalone, V. Bousson, S. Naili, C. Bergot, F. Peyrin, J.D. Laredo, G. Haiat, Anatomical distribution of the degree of mineralization of bone tissue in human femoral neck: impact on biomechanical properties, Bone 50 (10) (2012) 876–884.
[18] S.P. Kotha, N. Guzelsu, Mineralized collagen fibrils: a mechanical model with a staggered arrangement of mineral particles, Biophys. J. 79 (4) (2000) 1737–1746.
[19] S.P. Kotha, N. Guzelsu, The effects of interphase and bonding on the elastic modulus of bone: changes with age-related osteoporosis, Med. Eng. Phys. 22 (8) (2000) 575–585.
[20] V. Sansalone, T. Lemaire, S. Naili, Multiscale modelling of mechanical properties of bone: study at the fibrillar scale, C. R., Méc. 335 (8) (2007) 436–442.
[21] V. Sansalone, T. Lemaire, S. Naili, Variational homogenization for modeling fibrillar structures in bone, Mech. Res. Commun. 36 (2) (2009) 265–273.
[22] V. Sansalone, S. Naili, T. Lemaire, Nanostructure and effective elastic properties of bone fibril, Bioinsp. Biomim. Nanobiomater. 1 (3) (2012) 154–165.
[23] A. Clément, C. Soize, J. Yvonnet, Computational nonlinear stochastic homogenization using a non-concurrent multiscale approach for hyperelastic heterogeneous microstructures analysis, Int. J. Numer. Methods Eng. 91 (8) (2012) 799–824.
[24] C. Soize, Tensor-valued random fields for meso-scale stochastic model of anisotropic elastic microstructure and probabilistic analysis of representative volume element size, Probab. Eng. Mech. 23 (2–3) (2008) 307–323.
[25] S. Nemat-Nasser, M. Hori, Micromechanics: Overall Properties of Heterogeneous Materials, 2nd ed., Appl. Math. Mech., North-Holland, The Netherlands, 1999.
[26] P. Suquet (Ed.), Continuum Micromechanics, CISM Lecture Notes, vol. 377, Springer-Verlag, Wien, 1997.
[27] G. Jumarie, Maximum Entropy, Information Without Probability and Complex Fractals, Kluwer Academic Publishers, Dordrecht/Boston/London, 2000.
[28] J.N. Kapur, H.K. Kesavan, Entropy Optimization Principles with Applications, Academic Press, San Diego, 1992.
[29] A. Zaoui, Continuum micromechanics: survey, J. Eng. Mech. 128 (8) (2002) 808–816.
[30] J.D. Eshelby, The determination of the elastic field of an ellipsoidal inclusion, and related problems, Proc. R. Soc. A 241 (1226) (1957) 376–396.
[31] A.P. Suvorov, G.J. Dvorak, Rate form of the Eshelby and Hill tensors, Int. J. Solids Struct. 39 (21) (2002) 5659–5678.
[32] C. Hellmich, J. Barthelemy, L. Dormieux, Mineral-collagen interactions in elasticity of bone ultrastructure – a continuum micromechanics approach, Eur. J. Mech. A, Solids 23 (2004) 783–810.
[33] S. Lees, K.S. Prostak, V.K. Ingle, K. Kjoller, The loci of mineral in turkey leg tendon as seen by atomic force microscope and electron microscopy, Calcif. Tissue Int. 55 (3) (1994) 180–189.
[34] L. Arnold, Stochastic Differential Equations: Theory and Applications, John Wiley and Sons, New York, 1973.
[35] W. Feller, An Introduction to Probability Theory and Its Applications, John Wiley and Sons, New York, 1971.
[36] P. Halmos, Measure Theory, 2nd ed., Basics, vol. 1, Springer-Verlag, Berlin, 1976.
[37] P. Krée, C. Soize, Mathematics of Random Phenomena, Reidel, Dordrecht, 1986.
[38] M.G. Kendall, A. Stuart, The Advanced Theory of Statistics, vol. 3, Griffin, London, 1986.
[39] R.J. Serfling, Approximation Theorems of Mathematical Statistics, John Wiley and Sons, 1980.
[40] E.T. Jaynes, Information theory and statistical mechanics, Phys. Rev. 106 (4) (1957) 620–630.
[41] E.T. Jaynes, Information theory and statistical mechanics, Phys. Rev. 108 (2) (1957) 171–190.
[42] C. Shannon, A mathematical theory of communication, Bell Syst. Tech. J. 27 (1948).
[43] C. Soize, Maximum entropy approach for modeling random uncertainties in transient elastodynamics, J. Acoust. Soc. Am. 109 (5) (2001) 1979–1996.
[44] C. Soize, Non-Gaussian positive-definite matrix-valued random fields for elliptic stochastic partial differential operators, Comput. Methods Appl. Mech. Eng. 195 (1–3) (2006) 26–64.
[45] K. Macocco, Q. Grimal, S. Naili, C. Soize, Elastoacoustic model with uncertain mechanical properties for ultrasonic wave velocity prediction: application to cortical bone evaluation, J. Acoust. Soc. Am. 119 (2) (2006) 729–740.